

# Quantum Paramagnet and Frustrated Quantum Criticality in a Spin-One Diamond Lattice Antiferromagnet

Gang Chen<sup>1,2\*</sup>

<sup>1</sup>State Key Laboratory of Surface Physics, Department of Physics, Center for Field Theory & Particle Physics, Fudan University, Shanghai, 200433, P.R.China and

<sup>2</sup>Collaborative Innovation Center of Advanced Microstructures, Nanjing, 210093, P.R.China

(Dated: January 27, 2023)

Motivated by the very recent proposal of *topological quantum paramagnet* in the diamond lattice antiferromagnet  $\text{NiRh}_2\text{O}_4$ , we propose a minimal model to describe the magnetic interaction and properties of the diamond material with the spin-one local moments. The minimal model includes the first and second neighbor Heisenberg interactions as well as a local single-ion spin anisotropy that is allowed by the spin-one nature of the local moment and the tetragonal symmetry of  $\text{NiRh}_2\text{O}_4$  below 380K. We point out that there exists a quantum phase transition from a *trivial quantum paramagnet* when the single-ion spin anisotropy is dominant to the magnetic ordered states when the exchange is dominant. Due to the frustrated spin interaction, *extensively degenerate bosonic modes* emerge and become critical in the vicinity of the criticality, giving rise to unusual magnetic properties. Our phase diagram and experimental predictions for different phases provide a guideline for the identification of the ground state for  $\text{NiRh}_2\text{O}_4$ . Although our phase diagram and theoretical results are fundamentally different from the proposal of topological quantum paramagnet for  $\text{NiRh}_2\text{O}_4$ , it represents interesting possibilities for spin-one diamond lattice antiferromagnets.

**Introduction.**—The recent theoretical proposal of symmetry protected topological (SPT) ordered states has sparked a wide interest in the theoretical community [1–4]. The well-known topological insulator, that was proposed and discovered earlier, is a *non-interacting* fermion SPT protected by time reversal symmetry [5, 6]. In contrast, the SPTs in bosonic systems must be stabilized by the interactions [4]. The spin degrees of freedom with exchange interactions seem to be a natural candidate for realizing the boson SPTs [3]. In fact, the Haldane spin-one chain is a 1D boson SPT and is protected by the  $\text{SO}(3)$  spin rotational symmetry [7]. The realization of boson SPTs in high dimensions is still missing. It was speculated that, the spin-one diamond lattice antiferromagnet with frustrated spin interactions may host a topological quantum paramagnet that is a spin analogue of topological insulator and protected by time reversal symmetry [8]. Quite recently, a diamond lattice antiferromagnet  $\text{NiRh}_2\text{O}_4$  with  $\text{Ni}^{2+}$  spin-one local moments was suggested to fit into this proposal [9].

$\text{NiRh}_2\text{O}_4$  is a tetragonal spinel and experiences a structural phase transition from cubic to tetragonal at  $T = 380\text{K}$  [9]. As we show in Fig. 1, the magnetic ion  $\text{Ni}^{2+}$  has a  $3d^8$  electron configuration, forming a spin  $S = 1$  local moment and occupying the tetrahedral diamond lattice site. No signature of magnetic order was observed down to 0.1K in the magnetic susceptibility and specific heat measurements. Although this might fulfill the requirements for a topological quantum paramagnet, the more important time-reversal-protected gapless surface states are not observed. One may thus wonder if any alternative phase, that is distinct from topological quantum paramagnet, could provide a consistent experimental prediction with the current experiments. In this Letter, we propose a minimal spin model for  $\text{NiRh}_2\text{O}_4$

and study the full phase diagram and the phase transition of our model. We do not find the presence of the topological quantum paramagnet in our phase diagram. Instead, due to the strong spin frustration, the ordered state in our phase diagram can be easily destabilized and converted into a trivial quantum paramagnet by a moderate single-ion spin anisotropy. We predict that this seemingly trivial quantum paramagnetic state in a large parameter regime supports gapped magnetic excitation that develops *extensively degenerate band minima* in the

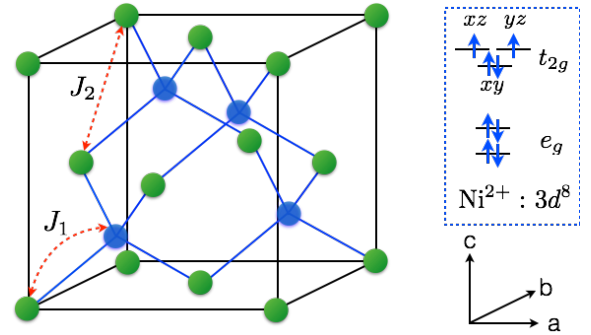


FIG. 1. (Color online.) The diamond lattice formed by the  $\text{Ni}^{2+}$  ions. The  $J_1$  and  $J_2$  interactions are indicated by (red) dashed arrows. Due to the tetragonal symmetry of the lattice, the  $a$  and  $b$  directions are not equivalent to the  $c$  direction. The  $\text{Ni}^{2+}$  ion is in a tetrahedral environment, so the  $e_g$  orbitals are lower in energy than the  $t_{2g}$  levels. The tetragonal distortion further splits the two  $e_g$  orbitals and the three  $t_{2g}$  orbitals. But the degeneracy of the  $xz$  and  $yz$  orbitals remains intact under the tetragonal distortion. To avoid the orbital degeneracy, we expect the  $xz$  and  $yz$  orbitals are higher in energy than the  $xy$  orbitals. The crystal field energy diagram and electron filling of the  $\text{Ni}^{2+}$  ion are depicted as the inset.

spectrum. As the quantum paramagnet approaches the phase transition to the proximate ordered state, the extensively degenerate low-energy modes become gapless and are responsible for the unusual magnetic properties such as the *linear- $T$  heat capacity* at low temperatures in the vicinity of the transition. In the proximate ordered phases, we further show that the spin spiral orders are actually induced by quantum fluctuations via quantum order by disorder.

*The microscopic spin model.*—To understand the interesting behaviors of  $\text{NiRh}_2\text{O}_4$ , we propose the following microscopic spin model,

$$H = J_1 \sum_{\langle \mathbf{r}\mathbf{r}' \rangle} \mathbf{S}_{\mathbf{r}} \cdot \mathbf{S}_{\mathbf{r}'} + J_2 \sum_{\langle\langle \mathbf{r}\mathbf{r}' \rangle\rangle} \mathbf{S}_{\mathbf{r}} \cdot \mathbf{S}_{\mathbf{r}'} + D_z \sum_{\mathbf{r}} (S_{\mathbf{r}}^z)^2, \quad (1)$$

where  $J_1$  and  $J_2$  are the first neighbor and second neighbor Heisenberg exchange interactions, respectively. Since the diamond lattice is a bipartite lattice, the first neighbor  $J_1$  interaction alone is unfrustrated, and would favor a simple Néel state if  $J_1$  is antiferromagnetic. The second neighbor interaction  $J_2$  is an interaction within each FCC sublattice of the diamond lattice. Due to the large numbers of second neighbor bonds, the  $J_2$  interaction would cause a spin frustration even when it is small compared to  $J_1$ . Previous classical treatment of the  $J_1$ - $J_2$  spin model on a diamond lattice and the analysis of thermal fluctuation have led to the interesting discovery of the spiral spin liquid [10, 11]. In our context, we will largely treat spins and interactions quantum mechanically. Moreover, an additional single-ion spin anisotropy is further introduced on top of the spin exchange interactions for  $\text{NiRh}_2\text{O}_4$ .  $\text{NiRh}_2\text{O}_4$  has a tetragonal lattice symmetry, so the three spin directions are not equivalent. The spin anisotropy is naturally allowed by the lattice symmetry and is the only term occurring for a spin-one local moment like the  $\text{Ni}^{2+}$  ion.

Due to this single-ion spin anisotropy, the magnetic susceptibilities along different directions should reveal such spin anisotropy. In particular, we carry out the high temperature series expansion and find that the Curie-Weiss temperatures for the magnetic field parallel and normal to the  $z$  direction are given as [12]

$$\Theta_{\text{CW}}^z = -\frac{D_z}{3} - \frac{S(S+1)}{3}(z_1 J_1 + z_2 J_2), \quad (2)$$

$$\Theta_{\text{CW}}^\perp = +\frac{D_z}{6} - \frac{S(S+1)}{3}(z_1 J_1 + z_2 J_2), \quad (3)$$

where  $z_1 = 4$  and  $z_2 = 12$  are the numbers of first neighbor and second neighbor bonds, respectively. The above prediction can be used to extract the single-ion spin anisotropy. Note for a powder sample, the Curie-Weiss temperature is  $\Theta_{\text{CW}}^{\text{Powder}} = -\frac{S(S+1)}{3}(z_1 J_1 + z_2 J_2)$  and is thus independent of the spin anisotropy.

*Quantum paramagnet and Phase diagram.*—To obtain the full phase diagram of the  $J_1$ - $J_2$ - $D_z$  model, we

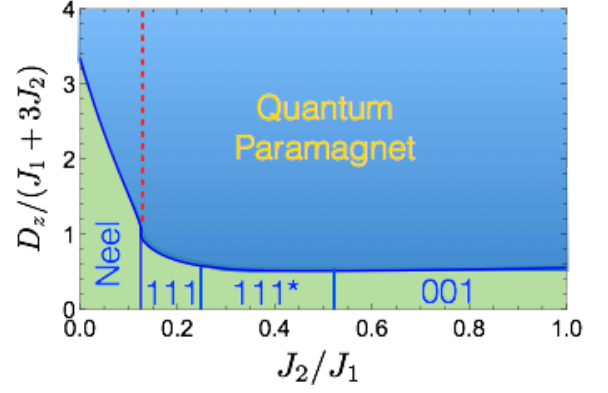


FIG. 2. (Color online.) The phase diagram of the  $J_1$ - $J_2$ - $D_z$  spin model. Because the powder sample Curie-Weiss temperature  $\Theta_{\text{CW}}^{\text{Powder}} = -8(J_1 + 3J_2)/3$ , we set the energy unit of the spin anisotropy  $D_z$  to  $J_1 + 3J_2$  in the plot. The transition from the quantum paramagnet to the ordered regions is continuous at the mean-field theory. On the left of the (red) dashed line, the band minimum of the magnetic excitation is unique and appears at  $\Gamma$  point. On the right side, the band minima form a degenerate surface in the reciprocal space. Please refer the main text for detailed discussion.

start from the parameter regime where the single-ion spin anisotropy is dominant. We consider the easy-plane anisotropy with  $D_z > 0$ , since the easy-axis spin anisotropy would stabilize the Néel state and enlarge its parameter regime. In the large and positive  $D_z$  limit, the ground state is a trivial quantum paramagnet with  $S^z = 0$  on every site,  $|\Psi\rangle = \prod_{\mathbf{r}} |S_{\mathbf{r}}^z = 0\rangle$ . For this simple state, there is no magnetic order and all the spin excitations are fully gapped. Since the global  $U(1)$  spin rotational symmetry around the  $z$  direction is preserved, the magnetic susceptibility at zero temperature for the field along the  $z$  direction is zero with  $\chi_z(T=0) = 0$ . However, if the field is applied in the  $xy$  plane, the spin rotational symmetry is broken by the in-plane field and the magnetic susceptibility is a constant with

$$\chi_\perp(T=0) = \frac{2\mu_0(g\mu_B)^2}{D_z + 2(z_1 J_1 + z_2 J_2)}, \quad (4)$$

where  $g$  is the Lande factor. Again, this result is a consequence of the single-ion anisotropy and can be used to detect the quantum paramagnetic state.

As we turn on the exchange interaction, the spin excitation would develop dispersion in the momentum space. With a sufficient exchange interaction, we expect the minimum of the dispersion to touch the zero energy that would lead to magnetic orderings. To describe the magnetic ordering transition out of the quantum paramagnetic phase, we substitute the spin operators with the rotor variables such that [13]

$$S_{\mathbf{r}}^z = n_{\mathbf{r}}, \quad S_{\mathbf{r}}^\pm = \sqrt{2}e^{\pm i\phi_{\mathbf{r}}}, \quad (5)$$

where  $\phi_{\mathbf{r}}$  is a  $2\pi$ -periodic phase variable and  $n_{\mathbf{r}}$  is integer-valued. This substitution has enlarged the physical

Hilbert space by allowing  $S^z$  or  $n$  to take the values beyond 0 and  $\pm 1$ . We, however, do not expect this approximation to cause significant effects since the non-physical values of  $n_r$  has been energetically suppressed by the large single-ion spin anisotropy. Moreover, the substitution preserves the global  $U(1)$  spin rotational symmetry around the  $z$  direction of the original spin model. Finally, to preserve the spin commutation relation, we impose the commutation for  $\phi_r$  and  $n_r$  with  $[\phi_r, n_{r'}] = i\delta_{rr'}$ .

With the rotor variables, the  $J_1$ - $J_2$ - $D_z$  spin model takes the form

$$H = J_1 \sum_{\langle rr' \rangle} [2 \cos(\phi_r - \phi_{r'}) + n_r n_{r'}] + J_2 \sum_{\langle\langle rr' \rangle\rangle} [2 \cos(\phi_r - \phi_{r'}) + n_r n_{r'}] + D_z \sum_r n_r^2. \quad (6)$$

From the symmetry point of view, the above model has the same symmetry as a standard boson Hubbard model except having an extra inter-site boson interaction. To make this analogy a little further, the quantum paramagnetic state is analogous to a boson Mott insulator with  $n_r = 0$  at every site, and the proximate magnetic order is like a superfluid of bosons. Despite the seemingly similarity, we will show below the intrinsic spin frustration brings rather interesting dispersion of magnetic excitation in the quantum paramagnet and thus leads to unusual properties at the analogous “superfluid-Mott” transition [14].

The primary operators that are responsible for the magnetic transition out of the quantum paramagnet are the  $S_r^\pm$  spin operators that create the gapped spin excitations in the quantum paramagnet but take finite values in the ordered states. We here carry out the coherent state path integral and integrate out the number operator  $n_r$ . The resulting partition function is

$$Z = \int \mathcal{D}\Phi_r \mathcal{D}\lambda_r \exp[-\mathcal{S} - \mathfrak{i} \sum_r \lambda_r (|\Phi_r|^2 - 1)], \quad (7)$$

where the effective action for the rotor variable is

$$\mathcal{S} = \int d\tau \sum_{\mathbf{k} \in \text{BZ}} (2D_z \mathbb{1}_{2 \times 2} + \mathcal{J}_{\mathbf{k}})^{-1} \partial_\tau \Phi_{i,\mathbf{k}}^\dagger \partial_\tau \Phi_{j,\mathbf{k}} + \sum_{\langle rr' \rangle} J_1 \Phi_r^\dagger \Phi_{r'} + \sum_{\langle\langle rr' \rangle\rangle} J_2 \Phi_r^\dagger \Phi_{r'}, \quad (8)$$

where we have introduced the variable  $\Phi_r \equiv e^{i\phi_r}$ . To impose the unimodular condition for  $\Phi_r$ , we have introduced a Lagrange multiplier  $\lambda_r$  on each site in Eq. (7). To solve for the dispersion of the excitation, we take a saddle point approximation and choose a uniform mean-field ansatz such that  $\mathfrak{i}\lambda_r \equiv \beta\Delta(T)$  where  $\beta = (k_B T)^{-1}$ . We integrate out the  $\Phi_r$  field and obtain the saddle-point

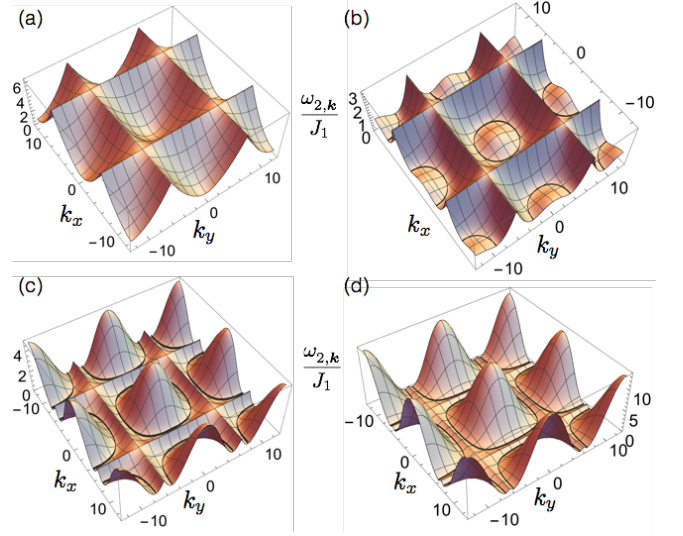


FIG. 3. (Color online.) The magnetic excitation  $\omega_{2,\mathbf{k}}$  in the  $k_x$ - $k_y$  plane of in the quantum paramagnet. We have chosen the following parameters (a)  $J_2 = 0.05J_1, D_z = 3J_1$ ; (b)  $J_2 = 0.18J_1, D_z = 1.5J_1$ ; (c)  $J_2 = 0.4J_1, D_z = 1.5J_1$ ; (d)  $J_2 = 0.8J_1, D_z = 2J_1$ . In the figure, we set  $k_z = 0$ , and an extended zone with  $k_x \in [-4\pi, 4\pi], k_y \in [-4\pi, 4\pi]$  is used. The degenerate minima are marked with contours. One can observe the evolution of the band minima.

equation for  $\Delta(T)$  in the quantum paramagnetic phase

$$\sum_{i=1,2} \sum_{\mathbf{k} \in \text{BZ}} \frac{2D_z + \xi_{i,\mathbf{k}}}{\omega_{i,\mathbf{k}}} \coth\left(\frac{\beta\omega_{i,\mathbf{k}}}{2}\right) = 2, \quad (9)$$

where  $\omega_{1,\mathbf{k}}$  and  $\omega_{2,\mathbf{k}}$  are the two modes of the magnetic excitations in the paramagnetic phase and are given by

$$\omega_{i,\mathbf{k}} = [(4D_z + 2\xi_{i,\mathbf{k}})(\Delta(T) + \xi_{i,\mathbf{k}})]^{\frac{1}{2}}, \quad (10)$$

and  $\xi_{1,\mathbf{k}}$  and  $\xi_{2,\mathbf{k}}$  are the two eigenvalues of the exchange matrix  $\mathcal{J}_{\mathbf{k}}$  [12]. As one decreases the single-ion spin anisotropy, the gap of the magnetic excitation decreases steadily. At the transition, the gap is closed and induces the magnetic order, and this phase transition is continuous within this treatment. In the phase diagram that is depicted in Fig. 2, the phase boundary between the quantum paramagnet and the magnetic order is then determined by examining the gap of the excitations in Eq. (10). In Fig. 2, the ordered region of the phase diagram is further split into several sub-regions with distinct magnetic orders from the quantum order by disorder effect. This will be explained below very soon.

*Frustrated quantum criticality.*—Here we point out the nontrivial magnetic excitation in the quantum paramagnetic state and the resulting frustrated quantum criticality. When  $J_2 < J_1/8$ , the band minimum of the lower excitation  $\omega_{2,\mathbf{k}}$  is at the  $\Gamma$  point. As we increase  $J_2$  beyond  $J_1/8$ , the dispersion minima are obtained by minimizing  $\xi_{2,\mathbf{k}}$ . We find that the minima of  $\omega_{2,\mathbf{k}}$  are extensively

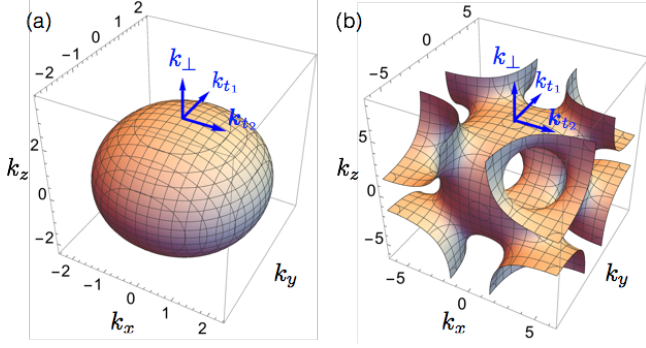


FIG. 4. (Color online.) The degenerate surface of the band minima at (a)  $J_2 = 0.18J_1$  and (b)  $J_2 = J_1/3$ . The  $(k_{t1}, k_{t2})$  are the two tangential momenta and  $k_\perp$  is the component normal to the degenerate surface.

degenerate and form a two-dimensional surface in the three-dimensional reciprocal space that is defined by

$$\cos \frac{k_x}{2} \cos \frac{k_y}{2} + \cos \frac{k_x}{2} \cos \frac{k_z}{2} + \cos \frac{k_y}{2} \cos \frac{k_z}{2} = \frac{J_1^2}{16J_2^2} - 1, \quad (11)$$

where we have set the lattice constant to unity. In Fig. 3, we depict the band  $\omega_{2,\mathbf{k}}$  in the  $k_x$ - $k_y$  plane with  $k_z = 0$ .

Now we explain how the behavior of the heat capacity in the vicinity of the magnetic critical point are modified by the large density of the low-energy excitations near the band minima. For  $J_2 < J_1/8$ , only a single bosonic mode becomes critical (see Fig. 3a) and leads to the usual  $C_v \propto T^3$  up to a logarithmic correction from the quantum fluctuation at the criticality. For  $J_2 > J_1/8$ , however, a *degenerate surface of bosonic modes* become critical at the transition (see Fig. 3b,c,d). To understand the consequence of this unusual phenomena, we return to the saddle point equation in Eq. (9) that reduces to

$$A \int_0^\Lambda dk_\perp \int_\Sigma d^2 \mathbf{k}_t \frac{\coth[\frac{\beta}{2}(m^2 + v^2 k_\perp^2)^{\frac{1}{2}}]}{(m^2 + v^2 k_\perp^2)^{\frac{1}{2}}} + c = 2, \quad (12)$$

where we have singled out the contribution from the critical modes as the first term in Eq. (12),  $A$  is an unimportant prefactor of the integration, and  $c$  is approximately  $T$ -independent contribution from the remaining part of the excitations. In Eq. (12), we have chosen the coordinate basis  $(\mathbf{k}_t, k_\perp)$  such that  $\mathbf{k}_t$  ( $k_\perp$ ) refer to the components of the momentum tange tangential to (normal to) the degenerate surface  $\Sigma$  (see Fig. 4), and  $\Lambda$  is the momentum cutoff. Here the critical mode behaves  $\omega_{2,\mathbf{k}} \simeq (m^2 + v^2 k_\perp^2)^{\frac{1}{2}}$  in which  $m$  is the thermally generated mass term and  $v$  is the velocity normal to the degenerate surface. At low temperatures ( $T \ll \Lambda$ ), the temperature dependent part of the integral becomes independent of the cutoff  $\Lambda$ , and only depends on  $T$  via the dimensionless parameter  $m^2/T^2$ . In order for the equality in Eq. (12) to hold, we expect  $m \propto T$ .

From the scaling form of  $m$ , we obtain a remarkable result for the low-temperature heat capacity that behaves as  $C_v \propto T$  at the criticality. This linear- $T$  heat capacity is like the one in a Fermi liquid metal, except that this is a pure bosonic system! This unusual behavior simply arises from the frustrated spin interaction.

*Quantum order by disorder.*—When the extensively degenerate modes are condensed at the critical point for  $J_2 > J_1/8$ , extensively degenerate candidate ordered states are available, and it is the quantum fluctuation of the spins that selects the the particular orders in the phase diagram of Fig. 2.

To explain this phenomenon, we first realize that the easy-plane spin anisotropy favors the magnetic order in the  $xy$  plane with

$$\mathbf{r} \in \text{A}, \quad \mathbf{S}_\mathbf{r} = S \text{Re}[(\hat{x} - i\hat{y})e^{i\mathbf{q} \cdot \mathbf{r}}], \quad (13)$$

$$\mathbf{r} \in \text{B}, \quad \mathbf{S}_\mathbf{r} = S \text{Re}[(\hat{x} - i\hat{y})e^{i\mathbf{q} \cdot \mathbf{r} + i\theta_\mathbf{q}}], \quad (14)$$

where  $\mathbf{q}$  is the propagating wavevector of the spin spiral, and  $\theta_\mathbf{q}$  is the phase shift between A and B sublattices of the diamond lattice. Both  $\mathbf{q}$  and  $\theta_\mathbf{q}$  can be obtained by a Weiss mean-field theory that is like the early classical treatment [10]. The quantum fluctuation with respect to the candidate spin spiral state is analyzed by a linear spin-wave theory and is discussed in the detail in the Supplementary information. As we plot in Fig. 2, quantum fluctuation favors the spiral wavevector to be either along [001] or [111] direction. For  $J_2 > J_1/4$ , the degenerate surface has expanded to the Brillouin zone boundary, and the [111] direction no longer intersects with the degenerate surface (see Fig. 4b as an example), the six points around the [111] direction are selected, and the resulting ordering states are labeled by [111\*] in Fig. 2.

*Discussion.*—In contrary to the proposal of a topological quantum paramagnet in  $\text{NiRh}_2\text{O}_4$  [9], our theoretical prediction does not support topological quantum paramagnet in our minimal  $J_1$ - $J_2$ - $D_z$  spin model. Instead, due to the strong frustrated spin interaction, a large region of trivial quantum paramagnet state is stabilized in the phase diagram. Although the trivial quantum paramagnet does not represent any new state of matter, the magnetic excitation is rather unusual and supports a degenerate surface of band minima in the spectrum. As the system is driven into a magnetic ordered state, extensively degenerate critical modes from the degenerate surface are condensed, leading to an unconventional critical properties at the transition.

To differentiate the proposal of topological quantum paramagnet and our proposal, we propose the following experiments. Topological quantum paramagnet supports gapless surface states that should be detectable by the surface thermal transport. Our prediction of the thermodynamic properties and the excitation spectrum for the trivial quantum paramagnet can be directly measured by the magnetic susceptibility and the inelastic neutron scattering. In the future, it is of interest to drive the



system close to the phase transition and directly access the critical properties.

*Acknowledgements.*—This work is supported by the Ministry of Science and Technology of People’s Republic of China with the Grant No.2016YFA0301001 (G.C.), the Start-Up Funds and the Program of First-class University Construction of Fudan University (G.C.), and the Thousand-Youth-Talent Program (G.C.) of People’s Republic of China. I thank Prof Nanlin Wang for the hospitality during my visit at ICQM of Peking University, Prof Zhong Wang for the hospitality during my visit at IAS of Tsinghua University, Prof Chen Fang for the hospitality during my visit at IOP, and Prof Ying Ran for the hospitality during my visit at Boston College this January when this work was motivated and finalized.

---

\* [gangchen.physics@gmail.com](mailto:gangchen.physics@gmail.com)

- [1] Xie Chen, Zheng-Cheng Gu, and Xiao-Gang Wen, “Classification of gapped symmetric phases in one-dimensional spin systems,” *Phys. Rev. B* **83**, 035107 (2011).
- [2] Xie Chen, Zheng-Cheng Gu, Zheng-Xin Liu, and Xiao-Gang Wen, “Symmetry protected topological orders and the group cohomology of their symmetry group,” *Phys. Rev. B* **87**, 155114 (2013).
- [3] Xie Chen, Zheng-Cheng Gu, and Xiao-Gang Wen, “Complete classification of one-dimensional gapped quantum phases in interacting spin systems,” *Phys. Rev. B* **84**, 235128 (2011).
- [4] Xie Chen, Zheng-Cheng Gu, Zheng-Xin Liu, and Xiao-Gang Wen, “Symmetry-protected topological orders in interacting bosonic systems,” *Science* **338**, 1604–1606 (2012).
- [5] M Zahid Hasan and Charles L Kane, “Colloquium: topological insulators,” *Reviews of Modern Physics* **82**, 3045 (2010).
- [6] Xiao-Liang Qi and Shou-Cheng Zhang, “Topological insulators and superconductors,” *Reviews of Modern Physics* **83**, 1057 (2011).
- [7] F.D.M. Haldane, “Continuum dynamics of the 1-D Heisenberg antiferromagnet: Identification with the O(3) nonlinear sigma model,” *Physics Letters A* **93**, 464 – 468 (1983).
- [8] Chong Wang, Adam Nahum, and T. Senthil, “Topological paramagnetism in frustrated spin-1 Mott insulators,” *Phys. Rev. B* **91**, 195131 (2015).
- [9] Juan Chamorro and Tyrel McQueen, “S = 1 on a Diamond Lattice in NiRh<sub>2</sub>O<sub>4</sub>,” APS March Meeting Abstract **B48.00006** (2017).
- [10] Doron Bergman, Jason Alicea, Emanuel Gull, Simon Trebst, and Leon Balents, “Order-by-disorder and spiral spin-liquid in frustrated diamond-lattice antiferromagnets,” *Nature Physics* **3**, 487–491 (2007).
- [11] Shang Gao, Oksana Zaharko, Vladimir Tsurkan, Yixi Su, Jonathan S White, Gregory S Tucker, Bertrand Roessli, Frederic Bourdarot, Romain Sibille, Dmitry Chernyshov, *et al.*, “Spiral spin-liquid and the emergence of a vortex-like state in MnSc<sub>2</sub>S<sub>4</sub>,” *Nature Physics* (2016).
- [12] Please see the supplementary information for the detailed

discussion.

- [13] Gang Chen, Michael Hermele, and Leo Radzihovsky, “Frustrated Quantum Critical Theory of Putative Spin-Liquid Phenomenology in 6H-B-Ba<sub>3</sub>NiSb<sub>2</sub>O<sub>9</sub>,” *Phys. Rev. Lett.* **109**, 016402 (2012).
- [14] Matthew P. A. Fisher, Peter B. Weichman, G. Grinstein, and Daniel S. Fisher, “Boson localization and the superfluid-insulator transition,” *Phys. Rev. B* **40**, 546–570 (1989).
- [15] This relation was previously obtained for the degenerate spin spiral of the classical treatment of  $J_1$ - $J_2$  model on the diamond lattice.

# Supplementary Information for “Quantum Paramagnet and Frustrated Quantum Criticality in a Spin-One Diamond Lattice Antiferromagnet”

- I. The magnetic susceptibility.
- II. Weiss mean-field theory in the quantum paramagnetic phase.
- III. Exchange matrix.
- IV. Quantum order by disorder.

## I. THE MAGNETIC SUSCEPTIBILITY

The presence of the single-ion anisotropy modifies the Curie-Weiss temperature. Since  $D_z > 0$  corresponds to the easy-plane spin anisotropy and tends to orient the spin in the  $xy$  plane, so we expect  $D_z$  to contribute an antiferromagnetic (ferromagnetic) Curie-Weiss temperature when the external field is applied along the  $z$  direction (in the  $xy$  plane). To examine this, here we carry out the high temperature expansion and extract the Curie-Weiss temperature. In a magnetic field that is applied along the  $z$  direction, the Hamiltonian is

$$H_h = \sum_{\mathbf{r}, \mathbf{r}'} J_{\mathbf{r}\mathbf{r}'} \mathbf{S}_{\mathbf{r}} \cdot \mathbf{S}_{\mathbf{r}'} + \sum_{\mathbf{r}} [D_z (S_{\mathbf{r}}^z)^2 - h S_{\mathbf{r}}^z]. \quad (15)$$

The magnetization  $M^z$  is then given as

$$M^z = \sum_{\mathbf{r}} \frac{\text{Tr}[S_{\mathbf{r}}^z e^{-\beta H_h}]}{\text{Tr}[e^{-\beta H_h}]}, \quad (16)$$

from which one can carry out the expansion in  $\beta = 1/(k_B T)$ . The linear order in  $\beta$  is the free ion contribution without the single-ion anisotropy  $D_z$ . For the second order terms in  $\beta$ , besides the usual contribution from the crossing term between the superexchange and the Zeeman coupling, we now have a new contribution from the crossing term between the single-ion anisotropy and the Zeeman coupling. These crossing terms make non-vanishing contributions to the magnetization. From the magnetization, it is straightforward to read the susceptibility and the Curie-Weiss temperature. Likewise, the magnetization and the Curie-Weiss temperature for the field in the  $xy$  plane can also be obtained.

## II. WEISS MEAN-FIELD THEORY IN THE QUANTUM PARAMAGNET

Here we explain the zero-temperature spin susceptibility in the quantum paramagnet. From a general symmetry point of view, the global U(1) spin rotational symmetry around the  $z$  direction is preserved in the quantum paramagnet, so the total  $S^z$  is a good quantum number and we can use the total  $S^z$  to label all the states. The quantum paramagnet is a *gapped* spin singlet state with

$\sum_{\mathbf{r}} S_{\mathbf{r}}^z = 0$ . Thus it is obvious that the spin susceptibility for field applied along  $z$  direction is zero.

For the magnetic field in the  $xy$  plane, the system no longer has a global U(1) symmetry, and the above argument fails. To calculate the zero-temperature spin susceptibility, we take a Weiss mean-field approach and replace the spin model with a mean-field model, *i.e.*,

$$H_x = \sum_{\mathbf{r}\mathbf{r}'} J_{\mathbf{r}\mathbf{r}'} \mathbf{S}_{\mathbf{r}} \cdot \mathbf{S}_{\mathbf{r}'} + \sum_{\mathbf{r}} [D_z (S_{\mathbf{r}}^z)^2 - h_x S_{\mathbf{r}}^x] \quad (17)$$

$\Downarrow$

$$H_{\text{MFx}} = \sum_{\mathbf{r}\mathbf{r}'} J_{\mathbf{r}\mathbf{r}'} S_{\mathbf{r}}^x \langle S_{\mathbf{r}'}^x \rangle + \sum_{\mathbf{r}} [D_z (S_{\mathbf{r}}^z)^2 - h_x S_{\mathbf{r}}^x] \quad (18)$$

where  $\langle S_{\mathbf{r}}^x \rangle \equiv m^x$  and we assume a uniform mean-field ansatz. We solve for  $m^x$  self-consistently and obtain the magnetization,

$$m^x = \frac{2h_x}{D_z + 2(z_1 J_1 + z_2 J_2)} \quad (19)$$

and the spin susceptibility

$$\chi_{\perp} = \frac{2\mu_0 (g\mu_B)^2}{D_z + 2(z_1 J_1 + z_2 J_2)}, \quad (20)$$

where we have put back in the physical units.

## III. EXCHANGE MATRIX

The exchange matrix, that was introduced in the main text, is simply obtained by Fourier transform of the exchange part of the Hamiltonian. We have

$$\mathcal{J}_{\mathbf{k}} = \begin{bmatrix} J_2 \sum_{\mu=1}^{12} e^{i\mathbf{k} \cdot \mathbf{b}_{\mu}} & J_1 \sum_{\mu=1}^4 e^{i\mathbf{k} \cdot \mathbf{a}_{\mu}} \\ J_1 \sum_{\mu=1}^4 e^{-i\mathbf{k} \cdot \mathbf{a}_{\mu}} & J_2 \sum_{\mu=1}^{12} e^{i\mathbf{k} \cdot \mathbf{b}_{\mu}} \end{bmatrix}, \quad (21)$$

where  $\mathbf{a}_{\mu}$  are the four first neighbor vectors and  $\mathbf{b}_{\mu}$  are the twelve second neighbor vectors.

The eigenvalues of  $\mathcal{J}_{\mathbf{k}}$  are easily obtained

$$\xi_{1,\mathbf{k}} = 4J_2 \alpha_{\mathbf{k}} + 2J_1 (1 + \alpha_{\mathbf{k}})^{1/2}, \quad (22)$$

$$\xi_{2,\mathbf{k}} = 4J_2 \alpha_{\mathbf{k}} - 2J_1 (1 + \alpha_{\mathbf{k}})^{1/2}, \quad (23)$$

where

$$\alpha_{\mathbf{k}} = \cos \frac{k_x}{2} \cos \frac{k_y}{2} + \cos \frac{k_x}{2} \cos \frac{k_y}{2} + \cos \frac{k_x}{2} \cos \frac{k_y}{2}. \quad (24)$$

#### IV. QUANTUM ORDER BY DISORDER

In the ordered regime, the system develops a spin spiral order in the  $xy$  plane, and the mean-field theory for the ordered state yields the mean-field Hamiltonian for the  $xy$  spin components,

$$H_{xy} = \frac{1}{2} \sum_{\mathbf{q}} \sum_{i,j} \mathcal{J}_{\mathbf{q},ij} (S_{i,\mathbf{q}}^x S_{j,-\mathbf{q}}^x + S_{i,\mathbf{q}}^y S_{j,-\mathbf{q}}^y). \quad (25)$$

The ordering wavevector  $\mathbf{q}$  and the phase shift  $\theta$  are determined by optimizing the eigenvalue and corresponding eigenvector of the exchange matrix. The optimal  $\mathbf{q}$  satisfies Eq. 11 and forms a degenerate surface when  $J_2 > J_1/8$ , and this result is consistent with the early classical treatment in Ref. 10. For the spin spiral state that is defined in Eqs. (13) and (14), the combined operation of the lattice translation and spin rotation around the  $z$  axis by the spiral angle remains to be a symmetry. We thus introduce the following Holstein-Primarkoff boson for the spin spiral state,

$$\mathbf{S}_{\mathbf{r}} \cdot \hat{n}_{\mathbf{r}} = S - a_{\mathbf{r}}^{\dagger} a_{\mathbf{r}}, \quad (26)$$

$$\mathbf{S}_{\mathbf{r}} \cdot \hat{z} = \frac{\sqrt{2S}}{2} (a_{\mathbf{r}} + a_{\mathbf{r}}^{\dagger}), \quad (27)$$

$$\mathbf{S}_{\mathbf{r}} \cdot (\hat{n}_{\mathbf{r}} \times \hat{z}) = \frac{\sqrt{2S}}{2i} (a_{\mathbf{r}} - a_{\mathbf{r}}^{\dagger}), \quad (28)$$

where  $\hat{n}_{\mathbf{r}}$  is the orientation of the spin spiral order at the lattice site  $\mathbf{r}$ . With this substitution of the spin operators, we obtain the linear spin-wave Hamiltonian that is given as

$$\begin{aligned} H_{\text{sw}} = & \sum_{\mathbf{k} \in \text{BZ}} (a_{1\mathbf{k}}^{\dagger}, a_{2\mathbf{k}}^{\dagger}, a_{1,-\mathbf{k}}, a_{2,-\mathbf{k}}) \\ & \times \begin{bmatrix} A_{\mathbf{k},11} & A_{\mathbf{k},12} & B_{\mathbf{k},11} & B_{\mathbf{k},12} \\ A_{\mathbf{k},12}^* & A_{\mathbf{k},22} & B_{-\mathbf{k},12} & B_{\mathbf{k},22} \\ B_{\mathbf{k},11}^* & B_{-\mathbf{k},12}^* & A_{-\mathbf{k},11} & A_{-\mathbf{k},12}^* \\ B_{\mathbf{k},12}^* & B_{\mathbf{k},22}^* & A_{-\mathbf{k},12} & A_{-\mathbf{k},22} \end{bmatrix} \begin{pmatrix} a_{1,\mathbf{k}} \\ a_{2,\mathbf{k}} \\ a_{1,-\mathbf{k}}^{\dagger} \\ a_{2,-\mathbf{k}}^{\dagger} \end{pmatrix} \\ & - \sum_{\mathbf{k} \in \text{BZ}} (A_{\mathbf{k},11} + A_{\mathbf{k},22}), \end{aligned} \quad (29)$$

where

$$\begin{aligned} A_{\mathbf{k},11} = A_{\mathbf{k},22} = & \frac{D_z}{2} - \frac{J_1}{2} \sum_{\mu=1}^4 \cos(\mathbf{q} \cdot \mathbf{a}_{\mu} + \theta) \\ & + \frac{J_2}{4} \sum_{\mu=1}^{12} [\cos(\mathbf{k} \cdot \mathbf{b}_{\mu}) + (\cos(\mathbf{k} \cdot \mathbf{b}_{\mu}) - 2) \cos(\mathbf{q} \cdot \mathbf{b}_{\mu})], \end{aligned} \quad (30)$$

$$A_{\mathbf{k},12} = \frac{J_1}{4} \sum_{\mu=1}^4 e^{i\mathbf{k} \cdot \mathbf{a}_{\mu}} [1 + \cos(\mathbf{q} \cdot \mathbf{a}_{\mu} + \theta)], \quad (31)$$

$$B_{\mathbf{k},11} = \frac{D_z}{2} + \frac{J_2}{4} \sum_{\mu=1}^{12} \cos(\mathbf{k} \cdot \mathbf{b}_{\mu}) [1 - \cos(\mathbf{q} \cdot \mathbf{b}_{\mu})], \quad (32)$$

$$B_{\mathbf{k},12} = \frac{J_1}{8} \sum_{\mu=1}^4 \cos(\mathbf{k} \cdot \mathbf{a}_{\mu}) [1 - \cos(\mathbf{q} \cdot \mathbf{a}_{\mu} + \theta)], \quad (33)$$

and  $a_{1,\mathbf{k}}$  and  $a_{2,\mathbf{k}}$  represent the Holstein-Primarkoff boson on the A and the B sublattices, respectively.

The spin-wave Hamiltonian is diagonalized by a Bogoliubov transformation. The quantum zero point energy is given as

$$\Delta E = \sum_{\mathbf{k}} \sum_{i=1}^2 \frac{1}{2} \Omega_{\mathbf{k},i} - \sum_{\mathbf{k}} 2A_{\mathbf{k},11}, \quad (34)$$

where  $\Omega_{\mathbf{k},i}$  is the  $i$ -th spin-wave mode at the momentum  $\mathbf{k}$ .

In the phase diagram in Fig. 2, the propagating wavevectors of the [111] spin spiral and the [001] spin spiral are uniquely specified by the intersection between the orientation and the degenerate surface. Here we describe the [111\*] spin spirals. As we have already pointed out in the main text, for  $J_2 > J_1/4$ , there is no intersection between the 111 axis and the degenerate surface. Instead, the Brillouin zone boundary/surface, that is normal to the 111 axis, intersects with the degenerate surface, and the interaction is a deformed circle (see Fig. 4b). The quantum fluctuation selects the propagating wavevector on this deformed circle. Due to the cubic symmetry, six equivalent wavevectors on the deformed circle are selected.